Earth and Space Science

RESEARCH ARTICLE
10.1029/2022EA002579

Modeling Coastal Water Clarity Using Landsat-8 and Sentinel-2

Sarah E. Lang[1,2], Kelly M. A. Luis[3,4], Scott C. Doney[1], Olivia Cronin-Golomb[1], and Max C. N. Castorani[1]

[1]Department of Environmental Sciences, University of Virginia, Charlottesville, VA, USA, [2]Graduate School of Oceanography, University of Rhode Island, Narragansett, RI, USA, [3]School for the Environment, University of Massachusetts Boston, Boston, MA, USA, [4]Jet Propulsion Laboratory, California Institute of Technology, Pasadena, CA, USA

Key Points:

- Coupled satellite estimates with in situ observations increased the spatiotemporal coverage of water clarity estimation in a coastal ocean lagoon system
- Demonstrated an accessible approach for modifying bio-optical algorithms in optically complex coastal waters
- Model improved water clarity estimates, reduced biases, and decreased errors associated with Landsat-8/Sentinel-2 differences

Supporting Information:

Supporting Information may be found in the online version of this article.

Correspondence to:

S. E. Lang,
slang@uri.edu

Citation:

Lang, S. E., Luis, K. M. A., Doney, S. C., Cronin-Golomb, O., & Castorani, M. C. N. (2023). Modeling coastal water clarity using Landsat-8 and Sentinel-2. *Earth and Space Science*, *10*, e2022EA002579. https://doi.org/10.1029/2022EA002579

Received 29 SEP 2022
Accepted 2 JUN 2023

Author Contributions:

Conceptualization: Sarah E. Lang, Scott C. Doney, Max C. N. Castorani
Data curation: Sarah E. Lang, Olivia Cronin-Golomb, Max C. N. Castorani
Formal analysis: Sarah E. Lang
Funding acquisition: Sarah E. Lang, Scott C. Doney, Max C. N. Castorani
Investigation: Sarah E. Lang
Methodology: Sarah E. Lang, Kelly M. A. Luis, Scott C. Doney, Olivia Cronin-Golomb, Max C. N. Castorani

Abstract Understanding and attributing changes to water quality is essential to the study and management of coastal ecosystems and the ecological functions they sustain (e.g., primary productivity, predation, and submerged aquatic vegetation growth). However, describing patterns of water clarity—a key aspect of water quality—over meaningful scales in space and time is challenged by high spatial and temporal variability due to natural and anthropogenic processes. Regionally tuned satellite algorithms can provide a more complete understanding of coastal water clarity changes and drivers. In this study, we used open-access satellite data and low-cost in situ methods to improve estimates of water clarity in an optically complex coastal water body. Specifically, we created a remote sensing water clarity product by compiling Landsat-8 and Sentinel-2 reflectance data with long-term Secchi depth measurements at 12 sites over 8 years in a shallow turbid coastal lagoon system in Virginia, USA. Our satellite-based model explained ~33% of the variation in in situ water clarity. Our approach increases the spatiotemporal coverage of in situ water clarity data and improves estimates from bio-optical algorithms that overpredicted water clarity. This could lead to a better understanding of water clarity changes and drivers to better predict how water quality will change in the future.

Plain Language Summary Water quality affects coastal ocean ecosystems and their ecological functions, including primary productivity, predation, and aquatic vegetation growth. An important component of water quality, water clarity, has historically been measured by tools such as Secchi disks. They are black and white painted disks that are lowered into the water column to estimate the depth at which they are no longer visible from the surface. They are a reliable, repeatable, and low-cost tool; thus, they have contributed to extensive long-term records of overall water quality. However, they produce gaps in space and time. Here, we created a remote sensing product to fill these gaps using open-access high resolution satellite data and low-cost in situ methods. Our product allows for the retrieval of water clarity data across an entire water body and at times field measurements are not available. This could lead to a better understanding of water clarity changes and drivers to better predict how water quality will change in the future.

1. Introduction

Measuring and predicting water quality variability is valuable for understanding and managing coastal marine and estuarine ecosystems (Álvarez-Romero et al., 2014). For example, understanding changes in water quality over space and time can aid the restoration and conservation of submerged aquatic vegetation, which is often limited by light availability (Carr et al., 2010). The health of coastal oceans are also tied to human well-being, with about 40% of the global population living within 100 km of the coast (Maul & Duedall, 2019). Coastal water quality impacts primary productivity and marine life, with associated impacts on fishing and industry (Cloern et al., 2014). Eutrophication, caused by an excess of nutrients and measured by changes in water quality metrics, can lead to hypoxia, harmful algal blooms, and fish kills (Sullivan et al., 2021).

Water clarity—a key component of water quality—has historically been measured using Secchi disks: black and white painted disks that are lowered into the water to estimate the depth at which they are no longer visible from the surface (Secchi depth [Z_{SD}]; Preisendorfer, 1986). Secchi disks serve as a reliable, repeatable, and low-cost tool; thus, they have contributed to extensive long-term records of overall water quality (Lee et al., 2015). For example, they are used by citizen scientists (Luis et al., 2019) to greatly expand sampling coverage, and in national assessments to measure water clarity as an ecological indicator for eutrophication (Sullivan et al., 2021).

Resources: Sarah E. Lang, Kelly M. A. Luis, Scott C. Doney, Max C. N. Castorani
Software: Sarah E. Lang, Kelly M. A. Luis, Olivia Cronin-Golomb
Supervision: Scott C. Doney, Max C. N. Castorani
Validation: Sarah E. Lang
Visualization: Sarah E. Lang
Writing – original draft: Sarah E. Lang
Writing – review & editing: Sarah E. Lang, Kelly M. A. Luis, Scott C. Doney, Max C. N. Castorani

However, due to logistical constraints, Z_{SD} and other in situ point measurements cannot fully capture broad-scale, long-term spatiotemporal variability in water clarity. Hence for most regions and time periods, there are large gaps in records of water clarity (Lee et al., 2016; Luis et al., 2019). Coupling remotely-sensed satellite measurements with in situ measurements could provide a more complete understanding of water quality changes and drivers in coastal ecosystems, as well as a way to separate directional trends from natural variability.

Z_{SD} and other biogeochemical parameters can be estimated by satellites measuring water-leaving radiances in the visible spectrum, referred to as "ocean color" (Lee et al., 2016; Werdell & McClain, 2019). Ocean color data can be helpful in studying coastal waters on a synoptic scale (>100 km^2), but coastal environments pose unique challenges to ocean color remote sensing; thus, most studies to link in situ and remotely sensed water clarity have been based in open ocean environments (Concha & Schott, 2016; Morel & Bélanger, 2006). High concentrations of particulate organic matter and suspended sediments, proximity to land, backscattering from shallow waters, and bubbles from breaking waves affect bio-optical measurements (Loisel et al., 2013). Validation with in situ measurements is crucial before implementing ocean color algorithms in any water body, but the unique challenges posed by the coastal zone make it especially important to develop and validate such algorithms.

A second challenge posed by satellite estimation of coastal water clarity is that the spatial resolution of traditional ocean color satellite sensors (≤1 km) is too coarse to avoid interference by landforms while capturing spatial variation across coastal waters features (e.g., river mouths, ocean inlets, coastal lagoons). Fortunately, the Landsat-8's Operational Land Imager (OLI) and the Sentinel-2's MultiSpectral Instrument (MSI) have moderate-to-high spatial resolution (10–60 m) that enable observations in coastal environments (Franz et al., 2015; Pahlevan et al., 2019). The benefit of combining these observations has been recently demonstrated. For example, NASA's Harmonized Landsat Sentinel (HLS)-2 project shows that using the two satellites in unison increases data accuracy and temporal resolution (Masek et al., 2018).

However, studies using Landsat 8 and Sentinel-2 to measure water clarity have largely focused on lakes and rivers, highlighting the need to evaluate product consistency in coastal seas (Chen et al., 2020; Manzo et al., 2015; Page et al., 2019). The Lee et al. (2015) semi-analytical Z_{SD} model has been applied to various water bodies, but cross comparisons of OLI and MSI have been limited in coastal seas and require further investigation for effective usage of satellite imagery for water quality monitoring (Chen et al., 2019; Lee et al., 2016; Liu et al., 2019; Luis et al., 2019).

Thus, this work evaluates the accuracy and consistency of Landsat-8 and Sentinel-2 water clarity estimates in a coastal ocean lagoon system in Virginia, USA. Satellite estimations of Z_{SD} estimates were compared with corresponding in situ Z_{SD} from long-term in situ sampling efforts and these comparisons informed the development of regionally tuned Z_{SD} models for Landsat 8 and Sentinel 2. These results reveal that regionally tuned satellite models can improve the estimation of overall water quality in shallow, turbid coastal areas.

2. Methods

2.1. Study System and In Situ Data Collection

We focused our investigation on a coastal lagoon system studied by the Virginia Coast Reserve (VCR) Long Term Ecological Research Project (VCR-LTER) located on the Eastern Shore of Virginia, USA, near the southern tip of the Delmarva Peninsula (Figure 1). The VCR is the largest expanse of undeveloped coastline along the U.S. Atlantic seaboard. Low nitrogen inputs and frequent exchange with the Atlantic Ocean via inlets between barrier islands (Figure 1) results in relatively good water quality in comparison with most temperate coastal bays and estuaries in the United States and worldwide (McGlathery et al., 2001). Due to low human impacts, the VCR serves as a model system for studying the long-term impacts of climate on temperate coastal lagoons. The VCR also serves as the site of a successful large-scale eelgrass restoration project, after a massive die-off in the early 1930s due to storms and disease (Reynolds et al., 2016). Water quality monitoring in the bay has informed restoration efforts and helped quantify positive environmental effects of restoration (Orth et al., 2020). Since 1992, VCR-LTER researchers have collected Z_{SD} and other water quality parameters at 17 sites that include tidal flats (0–2 m depth), deep flats (2–4 m depth), and deeper oceanic inlets and channels (>4 m depth) (McGlathery & Christian, 2020; Safak et al., 2015). Sampling was carried out monthly from 1998 to 2008, and quarterly from 2008 to 2021 (McGlathery & Christian, 2020). Temperature, salinity, and dissolved oxygen (converted to apparent oxygen utilization) were measured with a YSI Datasonde (6600 V2). Total suspended solids were estimated

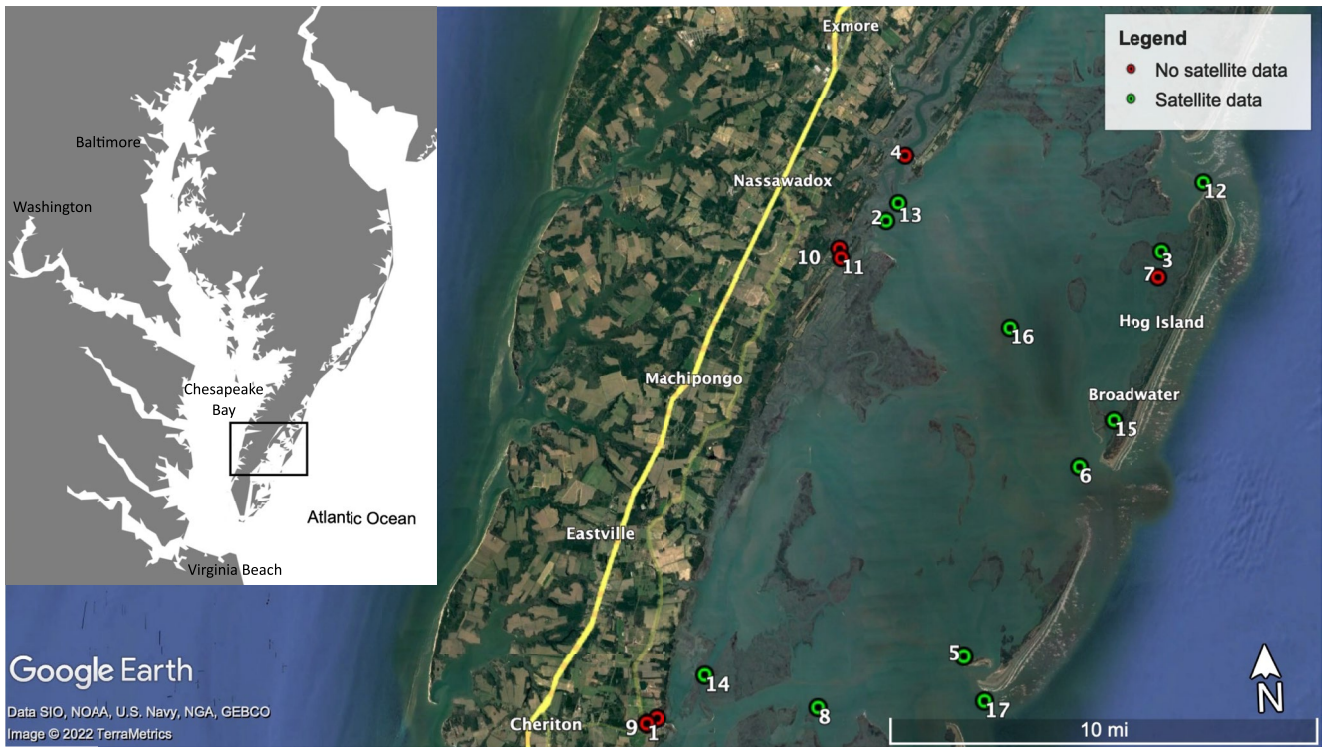

Figure 1. Map of the 17 tested sites with in situ Z_{SD} data. Numbers identify each site. Green markers indicate that satellite data could be collected at the site using the appropriate quality flags, while red markers indicate sites without valid satellite data.

via dry weight difference after filtering water samples with Whatman GF/F filters (0.7 μm nominal pore size), chlorophyll-a and phaeopigments were determined spectrophotometrically, and 500 mL water samples were analyzed for nutrient concentrations on a Lachat Quick-Chem 8500 flow-through analyzer.

2.2. Satellite Data Processing and Algorithm Evaluation

To retrieve remote sensing reflectances (R_{rs}) for the calculation of satellite-derived Z_{SD}, Landsat-8 and Sentinel-2 Level-1 images were collected. The Sentinel-2A and -2B satellites have a combined 5-day repeat orbit, while Landsat-8 has a 16-day repeat orbit. The OLI on Landsat-8 collects data at a 30 m spatial resolution in four spectral bands centered on wavelengths 443, 482, 561, and 655 nm. The MSI on Sentinel-2 collects data at 60 m spatial resolution with a band centered on 443 nm and at 10 m resolution for bands centered on 490, 560, and 665 nm. USGS Earth Explorer was used (U.S. Geological Survey, 2022; https://earthexplorer.usgs.gov/, accessed June 2019 through July 2022) to collect Level-1 Collection-1 Landsat-8 images (https://doi.org/10.5066/F71835S6) and the Copernicus Open Access Hub (European Space Agency, 2022; https://scihub.copernicus.eu/, accessed June 2020 through July 2022) to collect Level-1 Collection-1 Sentinel-2 images. The Landsat-8 and Sentinel-2 satellite images used in this study are listed as Tables S1 and S2 in Supporting Information S1, respectively.

R_{rs} were generated with two atmospheric correction processors: NASA's standard Level-2 generator atmospheric correction algorithm (l2gen) in NASA SeaDAS 8.2 (Baith et al., 2001) and ACOLITE from the Royal Belgian Institute of Natural Sciences (Version 20220222.0) (Vanhellemont, 2019, 2020; Vanhellemont & Ruddick, 2018). In l2gen, the NASA standard NIR-SWIR algorithm with bands 5 and 7 (865 and 2,201 nm) were selected for atmospheric correction of coastal waters (Wei et al., 2018). The following default Level-2 quality flags were used: CLDICE (probable cloud or ice contamination), HILT (very high or saturated radiance), and STRAYLIGHT (straylight contamination). LAND (pixel is over land) was deselected due to the default land mask being too coarse for this area and the following reflectance thresholds were used to flag and remove land pixels: $R_{rs}(655) < 0.01$, $R_{rs}(561) < 0.012$, $R_{rs}(482) < 0.001$, and $R_{rs}(443) < 0.001$. The bidirectional reflectance distribution function of Morel et al. (2002) was implemented. In ACOLITE, the default Dark Spectrum Fitting algorithm was implemented (Vanhellemont, 2019, 2020; Vanhellemont & Ruddick, 2018) with default masks for

land, negative reflectances, cirrus clouds, and high reflectance. Valid R_{rs} from l2gen and ACOLITE were recovered at 12 of 17 in situ sampling sites (five sites were too close to land): six ocean inlet sites, two lagoon sites, and three mainland tidal creek sites (Figure 1).

Z_{SD} was computed by deriving inherent and apparent optical properties from R_{rs}. The Quasi-Analytical Algorithm (QAA, version 6) was used to derive total absorption (a) and backscattering (b_b) coefficients from R_{rs} with the QAA (Lee et al., 2002), and these inherent optical property (IOP) coefficients were used to calculate the diffuse attenuation coefficient (K_d) with Lee et al., 2013. $K_d(530)$ was determined empirically by the methods of Lee et al. (2016) to fill the large spectral gap between 482 and 561 nm. The minimum K_d value, the spectral band with the lowest attenuation, and the R_{rs} value at the corresponding wavelength (R_{rs}^{tr}), were then used to compute the satellite derived Secchi depth ($Z_{SD,sat}$, m) (Equation 1) (Lee et al., 2015, 2016).

$$Z_{SD,sat} = \frac{1}{2.5\text{Min}\left(K_d^{tr}\right)} \ln\left(\frac{0.14 - R_{rs}^{tr}}{0.013}\right) \quad (1)$$

Satellite imagery within ±0–1 day of in situ sampling were used (2 OLI images, 6 MSI images) and $Z_{SD,sat}$ was found by averaging pixels in a 3 × 3 box (90 × 90 m for Landsat-8, 30 × 30 m for Sentinel-2) centered around the corresponding in situ site coordinate (Figure S1 in Supporting Information S1). The impact of anomalous data points on the spatial averaging within the 3 × 3 box was evaluated by also calculating the median of the 3 × 3 box. The mean and medians were not statistically different (Landsat-8: $P = 0.5$; Sentinel-2: $P = 0.9$). We did not filter for large variance due to limited match-ups, as is done in some studies using a coefficient of variation threshold (Dogliotti et al., 2011; Mélin, 2022). L2gen yielded 11 matchups from OLI and 41 matchups from MSI. ACOLITE yielded 3 OLI and 44 MSI matchups. The number of observations varied by site and date due to varying cloud cover and choice of quality flags. We removed matchups with recorded water depths within 0.5 m of the recorded in situ Secchi depths. The workflow is synthesized in Figure 2.

2.3. Cross Sensor Comparison

Landsat-8 and Sentinel-2 Secchi depths from l2gen and the Lee et al. (2016) algorithm ($Z_{SD,sat}$) (Equation 1) from the same day at the same location were compared. This approach yielded 5 clear-sky same-day images from 2021, from which we sampled 150 random coordinates using QGIS 3.14 (QGIS.org, 2020). We compared Landsat-8 $Z_{SD,sat}$ and Sentinel-2 $Z_{SD,sat}$ using a Type II ordinary least squares linear regression.

2.4. Modeling for Algorithm Adjustment

We used Type II ordinary least squares linear regression to predict in situ Secchi depths ($Z_{SD,insitu}$) from satellite Secchi depth estimates ($Z_{SD,sat}$) from l2gen and ACOLITE to determine which atmospheric correction software was most suitable. We also fit two individual linear models for Landsat-8 and Sentinel-2 data to determine whether Landsat-8 and Sentinel-2 differed in their predictions of in situ Z_{SD} and to determine the proportion of variance of in situ Z_{SD} explained by each satellite separately.

Models were fit in R 4.2.1 (R Core Team, 2022). We assessed the significance of model terms using F tests to determine if the model better fit the data than the Z_{SD} algorithm. We checked for homogeneity of variance by plotting normalized model residuals against model predictions and individual predictors. We ensured normality of residuals using histograms and quantile-quantile plots. We tested for temporal autocorrelation using autocorrelation function analysis; no significant autocorrelation was detected.

2.5. Model Assessment

We evaluated model skill by comparing modeled Secchi depths ($Z_{SD,model}$) to in situ Secchi depths ($Z_{SD,insitu}$) using the root mean square error (RMSE) and the mean absolute percent difference (MAPD) in R using the package *Metrics* 0.1.4 (Hamner & Frasco, 2018).

$$\text{RMSE} = \sqrt{\frac{1}{n}\sum_{i=1}^{n}\left(x_{\text{model},i} - x_{\text{in situ},i}\right)^2} \quad (2)$$

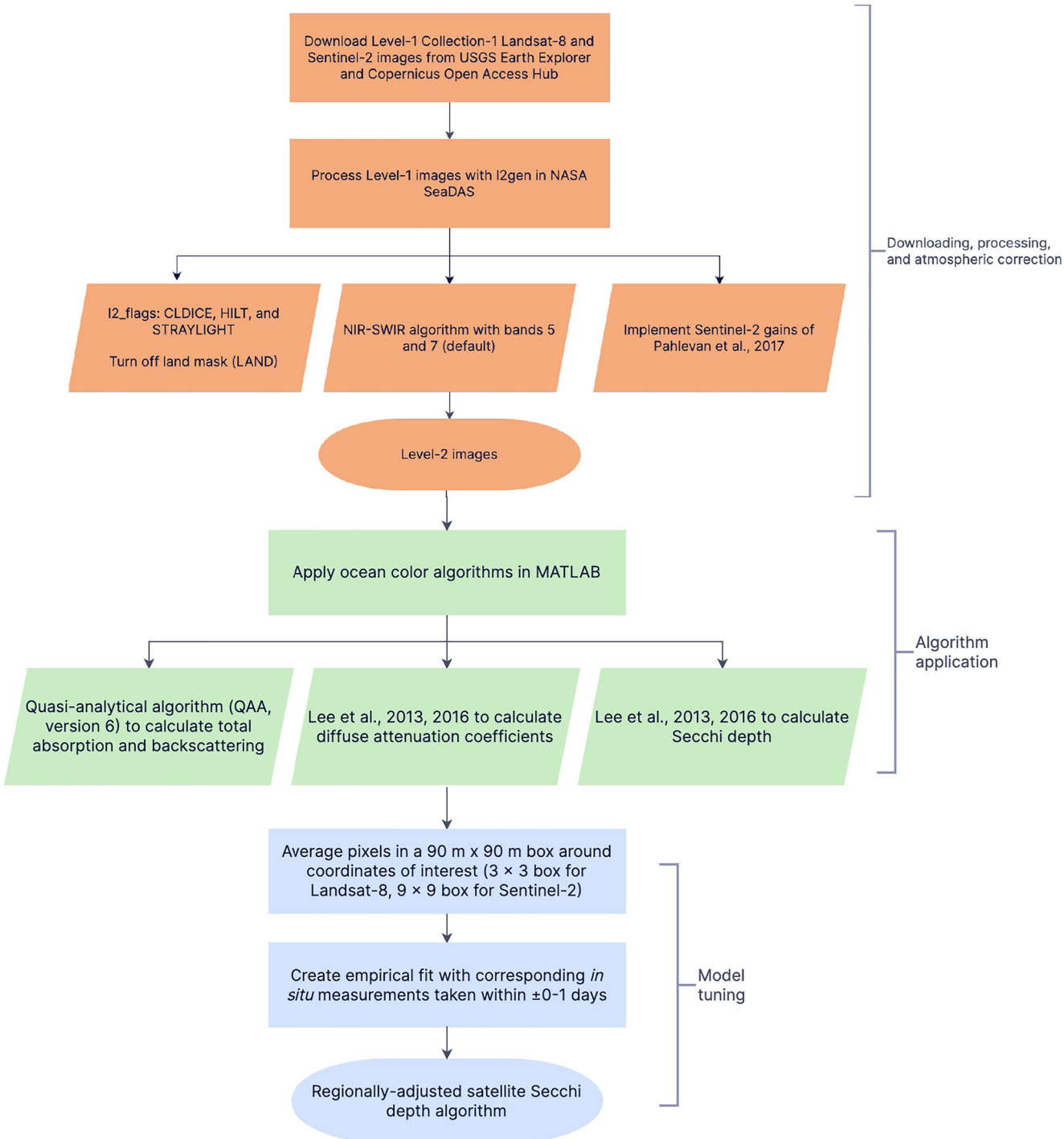

Figure 2. Workflow for obtaining Z_{SD} with l2gen in NASA SeaDAS, bio-optical algorithms, and empirical adjustments. l2gen ultimately chosen over ACOLITE for processing (Section 3.1).

$$\text{MAPD} = \frac{1}{n}\sum_{i=1}^{n}\left|\frac{x_{\text{model},i} - x_{\text{in situ},i}}{x_{\text{in situ},i}}\right| \times 100\% \quad (3)$$

Due to the lack of a sufficient number of observations for an out-of-sample validation, we assessed the uncertainty in the model coefficients by calculating the standard errors and confidence intervals with bootstrapping (n = 10,000) (R package *boot* 1.3–28; Canty & Ripley, 2021; Davison & Hinkley, 1997).

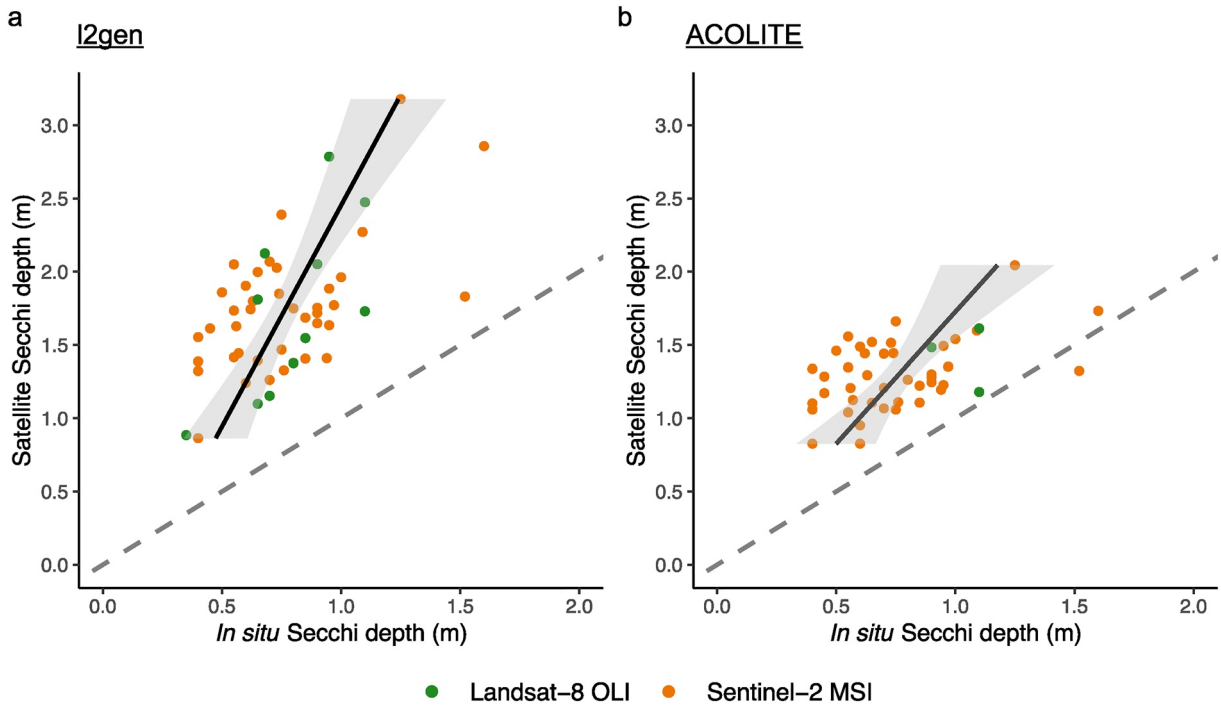

Figure 3. Z_{SD} predictions from l2gen (a) were generally greater than those from ACOLITE (b), although both were positively correlated with in situ measurements. Dotted line shows 1:1 relationship.

2.6. Spatiotemporal Analysis

We compared spatial trends of water clarity maps generated from clear sky Landsat-8 and Sentinel-2 images taken on the same day (30 January 2021). We also generated monthly water clarity maps from clear sky Landsat-8 images to demonstrate changing spatial patterns with time. To determine the benefit of increased temporal coverage, we visually compared temporal patterns in time series of combined satellite model estimates ($n = 396$ observations; 2013–2021) and all in situ data ($n = 306$ observations; 1992–2021) at three water quality sites in a lagoon (site 2), mainland creek (site 6), and ocean inlet (site 16). Specifically, generalized additive models (GAMs; Hastie & Tibshirani, 1986) were used to estimate nonlinear trends as a function of date (interannual variation), year-day (seasonal variation), and their interaction (tensor product) in R using the package *mgcv* 1.8–35 (Wood, 2017). By checking *k*-indices and *P* values, the following number of basis functions were selected: (a) 15 for date, (b) 15 for year day, and (c) 10 for the interaction/tensor product. Thin plate regression splines, computationally-efficient splines used to estimate smooth functions of multiple predictors, were used to model interannual variation and the interaction. We used cyclic cubic splines to model seasonal variation to avoid a discontinuity between the end and beginning of the year (Wood, 2017). To investigate seasonal trends in in situ water quality data, we used locally weighted scatterplot smoothing fits.

3. Results

3.1. Algorithm Evaluation

Satellite estimates overpredicted Z_{SD} relative to their corresponding in situ values by an average factor of about 2.4 for l2gen and 1.8 for ACOLITE. l2gen and ACOLITE Z_{SD} both predicted in situ Z_{SD} (l2gen: $R^2_{adj} = 32.5\%$, $F_{1,49} = 25.05$, $P < 0.001$; ACOLITE: $R^2_{adj} = 22.0\%$, $F_{1,43} = 13.38$, $P < 0.001$; Figure 3) and NASA l2gen yielded larger Z_{SD} from the Lee et al. (2016) algorithm (mean, $\overline{x} = 1.75$ m, standard deviation, $s = 0.46$ m) than ACOLITE ($\overline{x} = 1.30$ m, $s = 0.24$ m). However, ACOLITE still overpredicted Z_{SD} relative to the corresponding in situ values ($\overline{x} = 0.77$ m, $s = 0.26$ m).

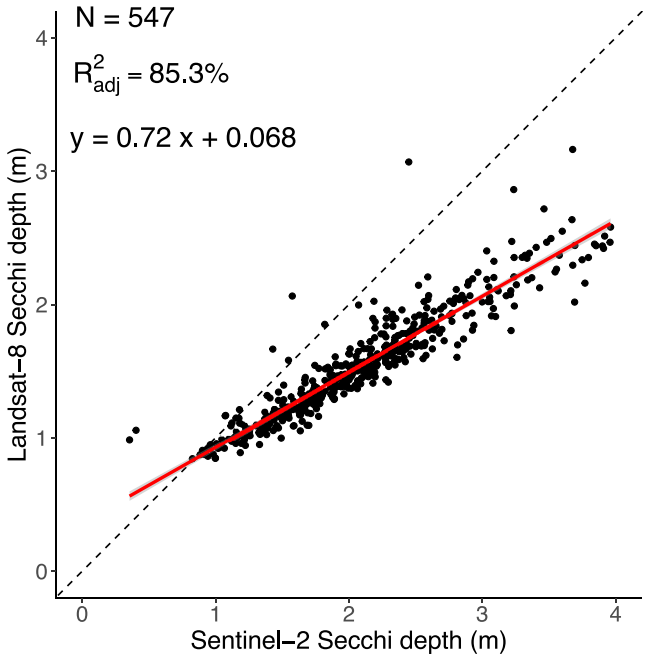

Figure 4. Landsat-8 $Z_{SD,sat}$ plotted against Sentinel-2 $Z_{SD,sat}$. Sentinel-2 generally yielded higher $Z_{SD,sat}$ than Landsat-8. Dashed 1:1 line as in Figure 3. Linear fit in red.

3.2. Cross-Sensor Comparisons

Z_{SD} estimates from the three satellites were highly correlated with a linear relationship (R^2_{adj} = 85.3%, $F_{1,545}$ = 3,170, $P < 0.001$). Sentinel-2 generally yielded higher $Z_{SD,sat}$ than Landsat-8 (note that most points are below the 1:1 line in Figure 4).

3.3. Model Statistics and Assessment

Spectral shapes were similar for both atmospheric correction processors, but ACOLITE systematically yielded larger R_{rs} than l2gen (Figure S2 in Supporting Information S1). Although ACOLITE yielded $Z_{SD,sat}$ that were closer to the 1:1 line ($Z_{SD,model}$ = 0.56 $Z_{SD,sat}$ + 0.04; Figure 3a) than l2gen $Z_{SD,sat}$ ($Z_{SD,model}$ = 0.33 $Z_{SD,sat}$ + 0.19; Figure 3b), R^2_{adj}, model skill metrics, and standard errors were better for the l2gen-based model (Table 1).

Due to differences in Landsat-8 and Sentinel-2 $Z_{SD,sat}$ estimates (Figure 4), the final algorithm adjustment involved separate satellite models (Equations 4 and 5). We also used l2gen atmospheric correction due to improved results over ACOLITE (Table 1).

$$\text{Landsat-8}: Z_{SD,model} = 0.25\, Z_{SD,sat} + 0.36 \quad (4)$$

$$\text{Sentinel-2}: Z_{SD,model} = 0.37\, Z_{SD,sat} + 0.10 \quad (5)$$

The final model (Equations 4 and 5; Figure 5) improved estimates (Landsat-8: RMSE = 0.16 m, MAPD = 19%; Sentinel-2: RMSE = 0.22 m, MAPD = 26%; Table 2) relative to the Lee et al. (2016) model (Landsat-8: RMSE = 1.04 m, MAPD = 121%; Sentinel-2: RMSE = 1.05 m, MAPD = 148%).

Model skill was similar among lagoon, mainland creek, and ocean inlet sites (Figure 6). There were no clear trends between water depth and model performance (Figure S3 and Table S3 in Supporting Information S1). Ocean inlet sites are most well-represented in the model, although the MSI model tends to underestimate high Z_{SD} at ocean inlet sites and overestimate low Z_{SD} (orange in Figure 6c).

3.4. Spatiotemporal Analysis

Spatial trends within the system were similar in Landsat-8 and Sentinel-2 water clarity maps taken on the same day, providing confidence that the remote sensing data is capturing robust geophysical and ecological patterns. Flows from the inlets through the deeper channels have higher Z_{SD} (ca. >0.8 m) than the surrounding water (ca. 0.4–0.7 m), and plumes off-shore of inlets have shallower Z_{SD} (0.6–0.8 m) than further offshore (>1 m). Sentinel-2 MSI had a larger Z_{SD} range (ca. 0.3–1 m) than Landsat-8 OLI (ca. 0.4–0.9 m) and captured finer scale spatial variability (Figure 7). Satellite images from individual dates highlight that Secchi depths in this system are highly variable in both time and space (Figure 8).

Table 1
Comparison of In Situ and Satellite Derived Z_{SD} From l2gen (SeaDAS) and ACOLITE

	l2gen (SeaDAS)	ACOLITE
RMSE	0.21 m	0.24 m
MAPD	25%	27%
Mean, standard error, and 95% CIs of the slope	0.33 ± 0.07 [0.22, 0.49]	0.56 ± 0.15 [0.29, 0.91]
Mean, standard error, and 95% CIs of the intercept	0.19 ± 0.11 [−0.08, 0.38]	0.04 ± 0.19 [−0.39, 0.37]
R^2_{adj}	32.5%	22.0%

Note. For each atmospheric correction method, the RMSE, MAPD, Mean, standard error, and 95% CIs of the intercept, and R^2_{adj} are reported.

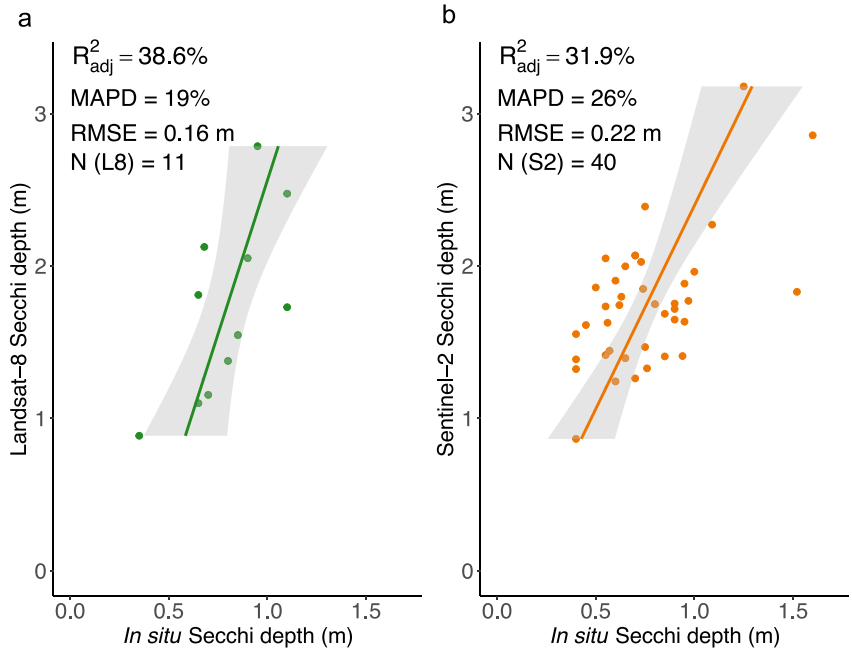

Figure 5. $Z_{SD,sat}$ from Landsat-8 (a) and Sentinel-2 (b) plotted against $Z_{SD,insitu}$. The single-satellite regression models (Equations 4 and 5) are plotted as solid lines with 95% confidence intervals plotted in gray.

Season cycles were significant at all three sites (Site 2: $P < 0.001$, Site 6: $P = 0.002$, Site 16: $P < 0.001$), as well as the tensor product explaining the interaction between interannual and seasonal variability (Site 2: $P = 0.006$, Site 6: $P = 0.009$, Site 16: $P = 0.01$; Figures 9a, 9c, and 9e). Sites 2 and 16 experienced the strongest seasonality and water clarity dips around July, corresponding to a dip in in situ Z_{SD} and peaks in in situ particulate inorganic matter, total suspended solids, apparent oxygen utilization, chlorophyll-a, phaeopigments, PO_4, and NH_4 (Figure 10). Interannual trends were not significant at any of the 3 sites (Site 2: $P = 0.20$, Site 6: $P = 0.66$, Site 16: $P = 0.26$; Figures 9b, 9d, and 9f).

4. Discussion

Landsat-8 and Sentinel-2 models were developed to increase and improve water clarity observations in the VCR-LTER. Our results demonstrate that high-resolution satellite observations can enable the estimation of water clarity in estuaries and coastal seas across a range of spatiotemporal scales, but require sensor-specific calibration and validation with in situ measurements. We anticipate that our approach can be adapted to coastal waters broadly where environmental monitoring organizations are limited to in situ data and potentially biased satellite estimates. The potential for high frequency water clarity estimation is further enhanced because we found that Landsat-8 and Sentinel-2 reflectances and Secchi depths are highly comparable.

Table 2
Model Skill Metrics, Model Uncertainties, and Fixed-Effects Results for Satellite Models

	Landsat-8 OLI (l2gen)	Sentinel-2 MSI (l2gen)
RMSE	0.16 m	0.22 m
MAPD	19%	26%
Mean, standard error, and 95% CIs of the slope	0.25 ± 0.092 [0.10, 0.48]	0.37 ± 0.094 [0.21, 0.58]
F, P value of the slope	$F = 7.30$, $P = 0.024$	$F = 19.22$, $P < 0.001$
Mean, standard error, and 95% CIs of the intercept	0.36 ± 0.16 [0.005, 0.64]	0.10 ± 0.16 [−0.25, 0.38]
F, P value of the intercept	$F = 4.74$, $P = 0.06$	$F = 0.44$, $P = 0.51$
Mean and standard error of R^2_{adj}	38.6% ± 22%	31.8% ± 14.5%

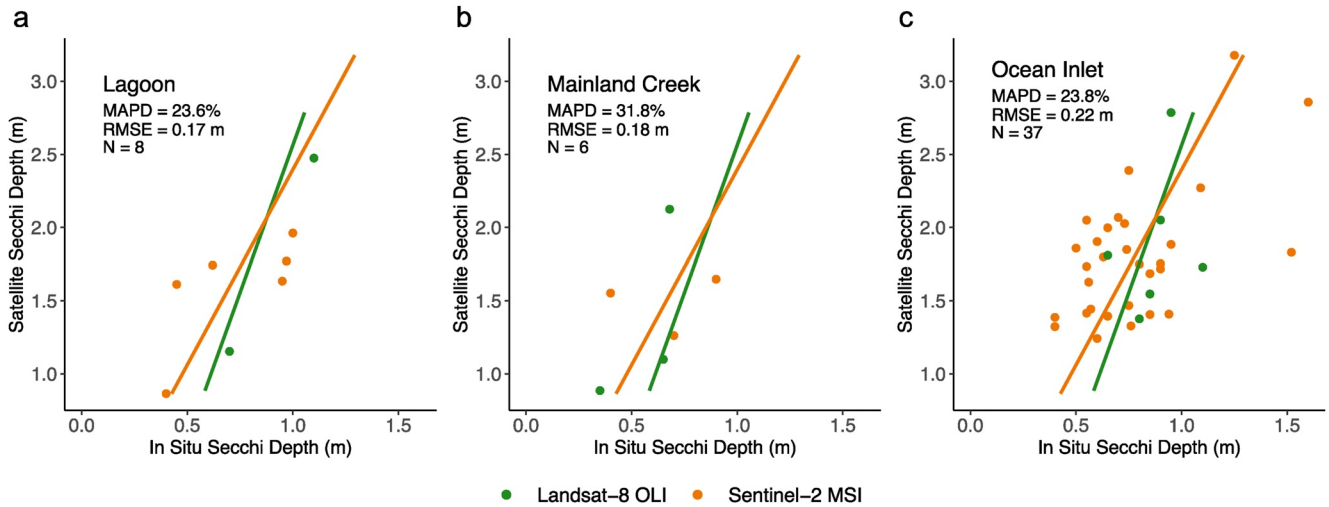

Figure 6. $Z_{SD,sat}$ from Landsat-8 (green) and Sentinel-2 (orange) plotted against $Z_{SD,insitu}$ for each site type. Sites no. 8 and 16 are lagoons, sites no. 2, 13, and 14 are mainland creeks, and sites no. 3, 5, 6, 12, 15, and 17 are ocean inlets. Landsat-8 (green) and Sentinel-2 (orange) prediction lines are plotted. Mean absolute percent difference (MAPD) and root mean square error (RMSE) are reported for each region. Sample size is not equal between site types.

4.1. Satellite Overestimation of Z_{SD}

Biases introduced during atmospheric correction could have led to satellite Z_{SD} overestimation. The atmospheric correction methods implemented by l2gen explained more variation in in situ Z_{SD} than ACOLITE (Figure 3, Table 1). This result complements previous work showing that l2gen performs better than ACOLITE for turbid waters and complex, optically shallow coastal environments (Ilori et al., 2019; Vanhellemont, 2019, 2020; Wei et al., 2018). We also found that ACOLITE consistently yielded higher reflectance values than l2gen at all four

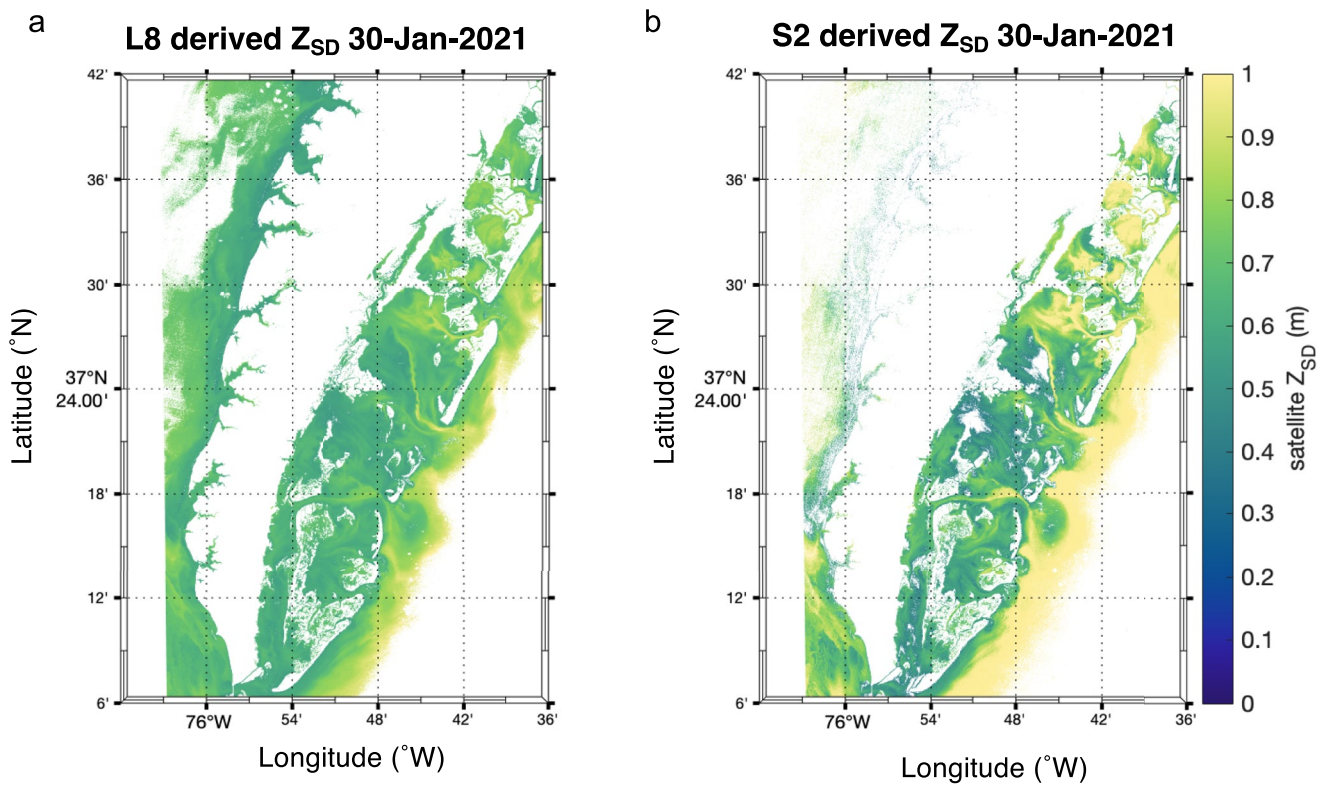

Figure 7. Maps of model-corrected Landsat-8 derived Z_{SD} (a) and Sentinel-2 derived Z_{SD} (b) from 30 January 2021.

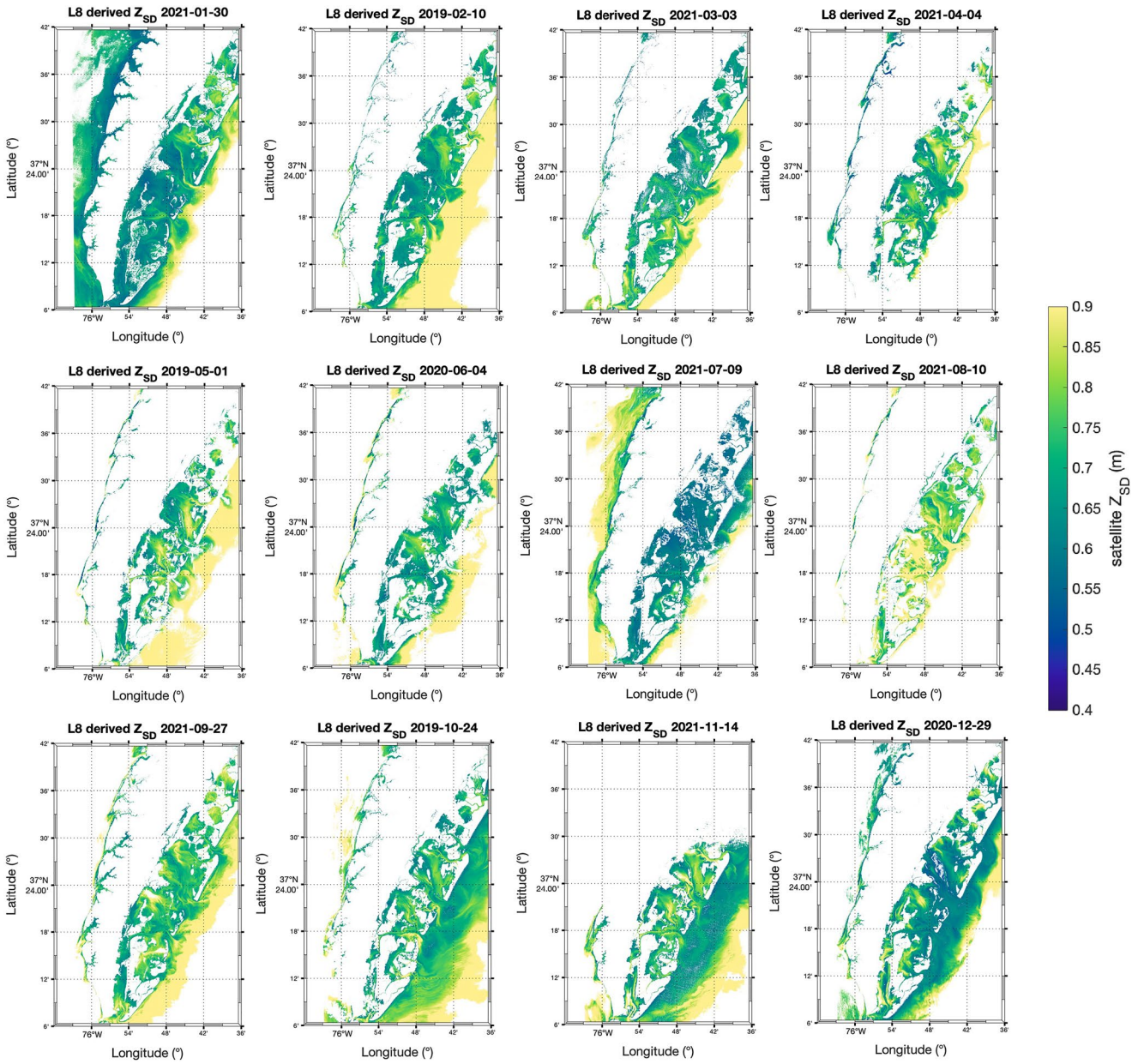

Figure 8. Maps of model-corrected Landsat-8 derived Secchi depths from monthly clear sky images (2019–2021).

wavelength bands (Figure S2 in Supporting Information S1). These results are consistent with the findings of Ilori et al. (2019) who compared different atmospheric correction methods over optically complex coastal waters using in situ radiometric measurements from the Aerosol Robotic Network—Ocean Color (AERONET-OC). Future work could investigate other atmospheric correction algorithms such as Case 2 Regional CoastColour (C2RCC) and POLYnomial-based algorithm applied to Medium Resolution Imaging Spectrometer (POLYMER) in this water body as was done in the Chesapeake Bay (Windle et al., 2022).

Validation of remote sensing products with in situ radiometric observations would be useful in regionally adjusting the algorithm. However, using an existing long-term data set for regional adjustment, as demonstrated in this paper, has its own advantages compared to this approach. Long term datasets have repeated seasonal sampling, so statistical models are less biased by the timing of in situ sampling. Capturing a wide range of variability in in situ sampling is especially important in systems that experience dynamic change across seasons. Using existing datasets is also cost effective compared to radiometric calibration. Another source of bias could have

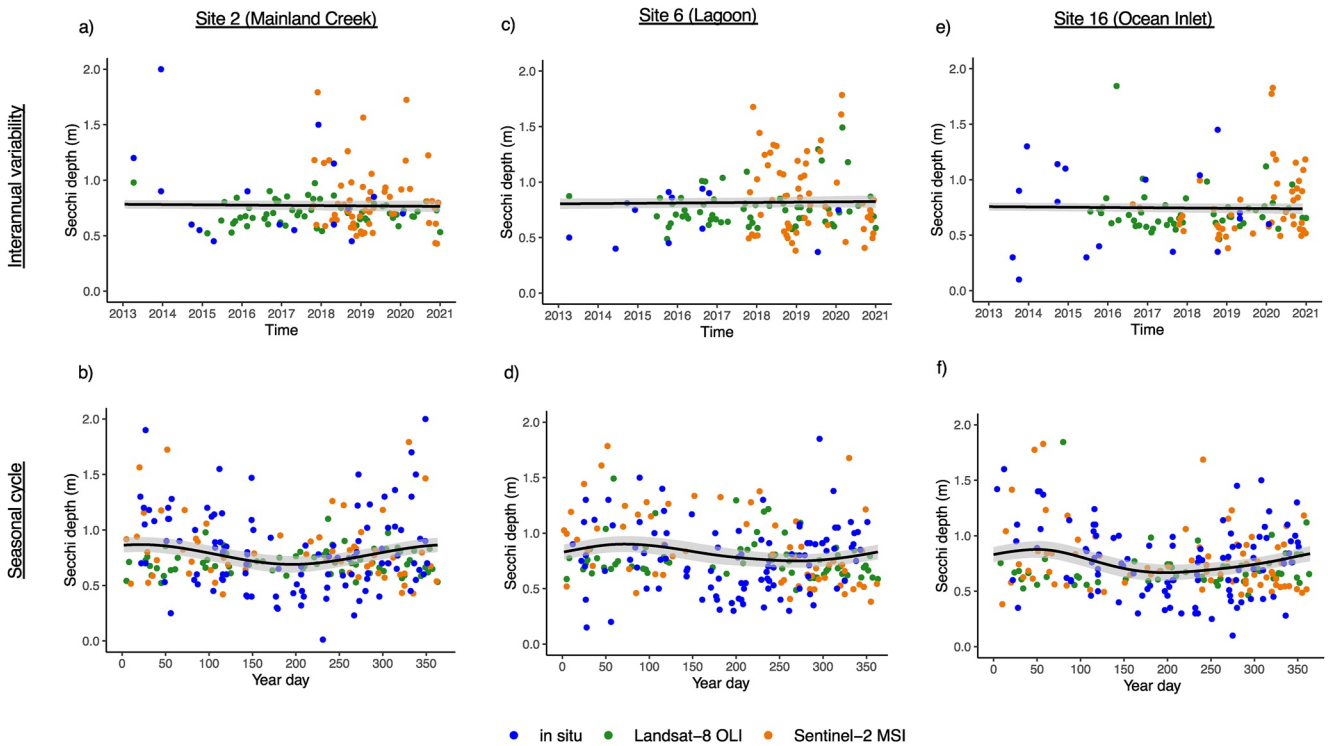

Figure 9. $Z_{SD,insitu}$ values (blue) and $Z_{SD,model}$ values (green: Operational Land Imager (OLI) and orange: MultiSpectral Instrument (MSI)) plotted against time (top; a, c, and e) and day of the year (bottom; b, d, and f) in a mainland creek (site 2; a–b), lagoon (site 6; c–d), and ocean inlet (site 16; e–f). Black lines show thin-plate regression splines and cyclic cubic splines for interannual (top) and seasonal (bottom) patterns from the generalized additive model, respectively. The splines were calculated from in situ, OLI, and MSI data. The 95% confidence intervals are plotted in gray.

been introduced during the derivation of IOPs. It has been found that the QAA can lead to underestimation of IOPs in turbid waters (Yang et al., 2014), which ultimately leads to an overestimation of $Z_{SD.}$ Alternative R_{rs} to IOP algorithms, such as the "QAA turbid" (Yang et al., 2014), or alternative Z_{SD} algorithms could possibly yield more accurate Z_{SD} values.

4.2. Using Sentinel-2 Data in Conjunction With Landsat-8 Data

The strong relationship between Landsat-8 and Sentinel-2 measurements (Figure 4) and similarities in spatial water clarity patterns (Figure 7) demonstrate the compatibility of their data products for estimating water clarity. We found that Sentinel-2 consistently yields larger Z_{SD} values (corresponding to lower R_{rs} values) than Landsat-8, suggesting that differences are most likely due to inherent satellite product differences rather than environmental factors (e.g., tidal differences occurring in the temporal window between satellite overpasses).

We decided to fit two separate models for each satellite due to differences in satellite estimates and to preserve the highest spatial resolution of Sentinel-2 MSI. However, care must be taken when comparing water clarity maps with different spatial resolutions. Down-sampling Sentinel-2 MSI to the spatial resolution of Landsat-8 OLI may be necessary for certain spatial analyses. Although down-sampling did not affect match-ups used in modeling (Figure S1 in Supporting Information S1), differences are significant when models are applied to entire satellite images (Figure 7).

Another consideration regarding merging Landsat and Sentinel data is parametrizing NASA's HLS products, surface reflectances with 30 m spatial resolutions and 5 days temporal resolutions (Masek et al., 2018). Although developed primarily for terrestrial applications, HLS data have been used in water quality modeling to increase temporal resolution while minimizing errors associated with satellite product differences (Peterson et al., 2020). The workflow for harmonizing products includes common atmospheric correction, spatial co-registration, normalization of the solar and view angles, and adjustment for differences in wave-

10.1029/2022EA002579

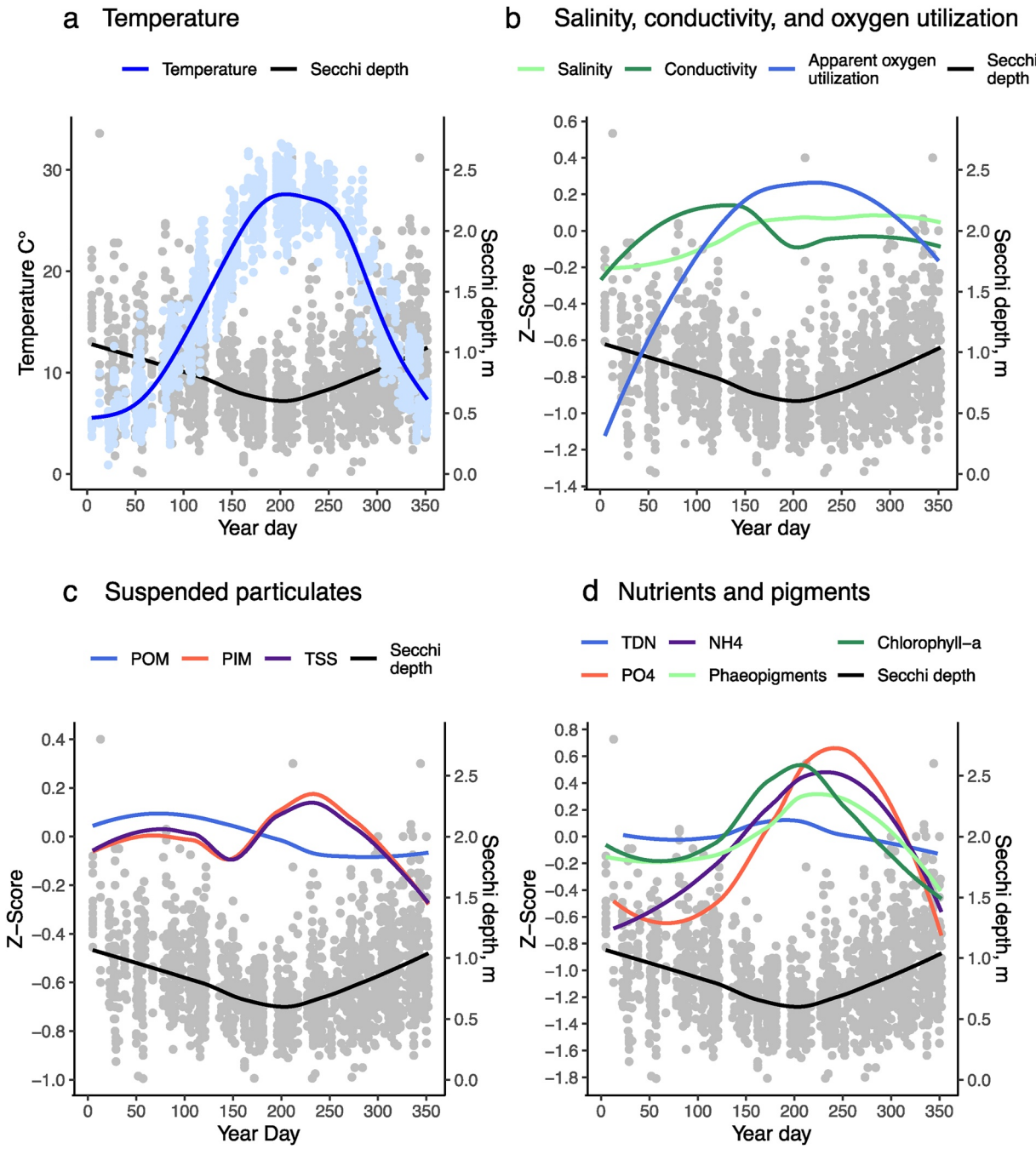

Figure 10. Seasonal trends in water quality parameters at 17 sites as shown by locally weighted scatterplot smoothing (LOWESS) fits. All parameters except Secchi depth and water temperature have been standardized. Panel A shows a peak in temperature (blue) corresponding to a dip in Secchi depth (black) mid-summer. Water temperature data are shown in light blue and Secchi depth data are shown in gray. Panels B–D show the seasonal variations of water quality parameters as modeled by LOWESS. Particulate organic matter denoted by POM, particulate inorganic matter denoted by PIM, total suspended solids denoted by TSS, and total dissolved nitrogen denoted by TDN. Secchi depths are plotted as well, as shown by the gray data points and black smooth. Data from 1992 to 2020 water quality sampling (McGlathery & Christian, 2020).

length bands (Claverie et al., 2018). This procedure corrects for Landsat-8/Sentinel-2 differences that could have contributed to the mismatch between Landsat-8 and Sentinel-2 reflectances and Secchi depths in our study.

4.3. Data Collection and Model Limitations

Our work highlights the need for in situ bio-optical and water quality measurements to fully leverage satellite imagery as an effective and reliable water quality monitoring tool, especially in dynamic waters. Increasing the number of in situ match-ups, especially to cover a large dynamic range, will strengthen the predictive power of statistical water clarity models. In this study, in situ sites were limited to the area shown in Figure 1. Application of the satellite model (adjustment to standard water clarity algorithm) outside of the VCR-LTER region and conditions introduces potential uncertainties. This could be addressed in future work by expanding the spread of in situ evaluation sites to quantify the accuracy of the model outside this region.

Although both satellites capture similar spatial patterns (Figure 7), the Sentinel-2 model captures higher Secchi depth values than the Landsat-8 model. We had limited in situ data for Landsat-8 adjustment due to its infrequent overpass relative to Sentinel-2. The discrepancy could be due to the inclusion of high (>1 m) in situ Secchi depths in the Sentinel-2 model. Although we captured a sufficient range of Secchi depths for a statistical fit, the Landsat-8 model would be strengthened by adding higher in situ Secchi depth values (>1 m). Coordinating field surveys with satellite overpasses would strengthen future remote sensing studies and provide more matchups for empirical algorithm adjustments.

Additionally, further investigation into the diurnal variability introduced by tidal forcing is important for interpreting water clarity (Shi et al., 2013). Future work could expand on our model to include tidal effects, which are different at each site. The residence times in this system range from weeks near the mainland to hours near the inlets (Safak et al., 2015), so tides more significantly affect inlet match-ups. We recommend that the current model be used to map spatiotemporal patterns and changes in water clarity across Landsat and Sentinel sensors.

4.4. Coupled In Situ/Satellite Spatiotemporal Analysis

Spatial variation in water clarity as captured by MSI and OLI (Figures 7 and 8) is affected by aquatic vegetation, salt marshes, tides, winds, bathymetry, and other factors. Submerged aquatic vegetation decreases turbidity by enhancing sediment deposition, and salt marshes (masked in white) slow down exchange with the ocean (Nardin et al., 2018). Strong winds can lead to increased mixing in the lagoon and decreased lagoon/ocean exchange (Safak et al., 2015). Patterns in water clarity can be paired with other data (e.g., bathymetry, weather data, hydrology) to better understand drivers of water clarity.

Satellite Z_{SD} maps (Figure 8) and in situ water quality data (Figure 10) demonstrate strong temporal variability in Secchi depth. As a highly seasonal system, we expect water clarity to change over the course of the year, but trends shown by in situ or satellite data alone may be affected by unique biases introduced by each approach. Field measurements are rarely taken during stormy winter weather when the water is more mixed and turbid, so in situ winter values may be biased toward higher measurements. In situ Z_{SD} depth measurements can also be biased by reduced visibility from waves, cloud cover, and sun position, as well as observer error (Pitarch, 2020). Satellite measurements are also imperfect, being affected by adjacency effects, proximity to land, seafloor backscatter, cloud cover, and aliasing due to whitecaps. There are also spatial limitations in satellite data retrievals, as shown by the inability to obtain satellite data too close to land (ca. <100 m away) or in areas affected by sunglint.

Coupling in situ Z_{SD} with satellite Z_{SD} can help alleviate these biases. For example, satellite data in our temporal analysis of three representative water quality sites may have alleviated the wintertime bias in in situ measurements. Additionally, the timing of field sampling within a season changed among years, which may have led to seasonal trends being confounded with interannual variability. Satellite data from 2013 to 2021 helped fill these gaps and create a more even spread of data across the year (Figures 9b, 9d, and 9f). An area for future work would be to conduct a rigorous analysis of Secchi depth seasonality using paired in situ and satellite observations. Interannual in situ Z_{SD} were also scarce at all three sites from 2013 to 2021 before satellite data was added. The combined time series showed no evidence of interannual changes, although relative constancy in water clarity may soon be changing (Parker & Crichton, 2011). This provides opportunities to further evaluate the model's predictive power with future in situ matchups. Rapid, accelerating sea level rise (Sallenger et al., 2012) and storm intensification (Fenster & Hayden, 2007; Hayden et al., 1991) may increase coastal erosion and increase turbidity (Turner et al., 2021). Likewise, increasing frequency, duration, and intensity of marine heatwaves threaten recently restored seagrass meadows, which have stabilized sediments and reduced local turbidity and chlorophyll concentrations (Aoki et al., 2020; Orth et al., 2012; Ummenhofer & Meehl, 2017). Rising water temperatures could also

affect numerous parameters relevant to water clarity such as phytoplankton concentrations (Pesce et al., 2018; Trombetta et al., 2019). It is vital to couple in situ observations with satellite observations over the long term to understand and derive changes in water clarity and separate directional trends from natural variability.

5. Conclusion

We developed a Landsat-8/Sentinel-2 remote sensing model to estimate water clarity in an optically complex coastal water body. The application of this model increases the spatiotemporal resolution of water clarity estimation, addresses algorithm overestimates of water clarity for specific localities, and decreases errors associated with Landsat-8/Sentinel-2. We believe our approach can be implemented in dynamic coastal water bodies with limited in situ measurements; for example, as part of routine water quality monitoring. Coupling accurate satellite estimates with in situ observations over the long term is crucial to understanding coastal water clarity variability and its underlying physical and biological drivers. This understanding could help improve water clarity predictions and lead to the better management of coastal ecosystems.

Data Availability Statement

Datasets and software used for the analysis of in situ and satellite data were archived with the Environmental Data Portal (EDI) via https://doi.org/10.6073/pasta/fe66683665a0133b2d831e552ecbae10 under a CC-BY Attribution license and are available in this in-text citation reference: Lang et al. (2022). Satellite data was processed by NASA SeaDAS 8.2 (Baith et al., 2001; National Aeronatics and Space Administration and Ocean Biology Processing Group, 2022), available for download at https://seadas.gsfc.nasa.gov/downloads/ under the GNU General Public License (GPL), and ACOLITE from the Royal Belgian Institute of Natural Sciences (Version 20220222.0) (Royal Belgian Institute of Natural Sciences and The Remote Sensing and Ecosystem Modelling Team, 2022; Vanhellemont, 2019, 2020; Vanhellemont & Ruddick, 2018), available for download at https://odnature.naturalsciences.be/remsem/software-and-data/acolite under the GNU General Public License v2. Level-1 Collection 1 Landsat-8 were downloaded from USGS Earth Explorer, available here: https://earthexplorer.usgs.gov (U.S. Geological Survey, 2022) in compliance with U.S. Public Domain. Level-1 images used in this study can be downloaded using the bounding box [37.6501, −75.7864], [37.6077, −75.4582], [37.0596, −75.7809], [37.1570, −76.0776], date range 1 January 2013 to 30 July 2022, and Landsat Level-1 Collection-1 under Data Sets. Level-1 Collection-1 Sentinel-2 images are available to download from the Copernicus Open Access Hub (European Space Agency, 2022), available here: https://scihub.copernicus.eu/ and subject to the Legal Notice on the use of Copernicus Sentinel Data and Service Information: https://sentinels.copernicus.eu/documents/247904/690755/Sentinel_Data_Legal_Notice. Level-1 data used in this study can be downloaded by selecting the appropriate bounding box around the VCR peninsula (see above coordinates), selecting Sentinel-2 mission, and selecting S2MSI1C as the Product Type. Processed Level-2 imagery available at Lang et al., 2022 data set described above. In situ water quality data is available at this in-text citation reference: McGlathery and Christian (2020) and at http://www.vcrlter.virginia.edu/cgi-bin/showDataset.cgi?docid=knb-lter-vcr.247 under a CC-BY Attribution license. Random sampling of coordinate points was done in QGIS 3.14 (QGIS.org, 2020) at https://www.qgis.org/en/site/forusers/download.html and under the GNU General Public License (GPL). Figures and statistics were done in R 4.2.1 (R Core Team, 2022) at https://www.qgis.org/en/site/forusers/download.html and under the GNU General Public License v2. Satellite algorithms were applied in MATLAB (The MathWorks, Inc., 2022) at https://www.mathworks.com/products/matlab.html.

Acknowledgments

We thank the numerous scientists, technicians, and students involved over the years in the water quality sampling and analysis component of the Virginia Coast Reserve LTER program. Early elements of this study were conducted by Jacob Bushey as part of undergraduate research at the University of Virginia. This work was funded by The Virginia Space Grant Consortium (award GG12317) with additional support from the National Science Foundation (NSF award 1832221).

References

Álvarez-Romero, J. G., Wilkinson, S. N., Pressey, R. L., Ban, N. C., Kool, J., & Brodie, J. (2014). Modeling catchment nutrients and sediment loads to inform regional management of water quality in coastal-marine ecosystems: A comparison of two approaches. *Journal of Environmental Management*, *146*, 164–178. https://doi.org/10.1016/j.jenvman.2014.07.007

Aoki, L. R., McGlathery, K., Wiberg, P., & Al-Haj, A. N. (2020). Depth affects seagrass restoration success and resilience to marine heat wave disturbance. *Estuaries and Coasts*, *43*(2), 316–328. https://doi.org/10.1007/s12237-019-00685-0

Baith, K., Lindsay, R., Fu, G., & McClain, C. R. (2001). Data analysis system developed for ocean color satellite sensors. *Eos, Transactions American Geophysical Union*, *82*(18), 202. https://doi.org/10.1029/01EO00109

Canty, A., & Ripley, B. (2021). boot: Bootstrap R (S-Plus) functions. R package version1.3-28.

Carr, J., D'Odorico, P., McGlathery, K., & Wiberg, P. (2010). Stability and bistability of seagrass ecosystems in shallow coastal lagoons: Role of feedbacks with sediment resuspension and light attenuation. *Journal of Geophysical Research*, *115*(G3), G03011. https://doi.org/10.1029/2009JG001103

Chen, J., Han, Q., Chen, Y., & Li, Y. (2019). A Secchi depth algorithm considering the residual error in satellite remote sensing reflectance data. *Remote Sensing*, *11*(16), 1948. https://doi.org/10.3390/rs11161948

Chen, J., Zhu, W., Tian, Y. Q., & Yu, Q. (2020). Monitoring dissolved organic carbon by combining Landsat-8 and Sentinel-2 satellites: Case study in Saginaw River estuary, Lake Huron. *Science of the Total Environment*, *718*, 137374. https://doi.org/10.1016/j.scitotenv.2020.137374

Claverie, M., Ju, J., Masek, J. G., Dungan, J. L., Vermote, E. F., Roger, J.-C., et al. (2018). The harmonized Landsat and Sentinel-2 surface reflectance data set. *Remote Sensing of Environment*, *219*, 145–161. https://doi.org/10.1016/j.rse.2018.09.002

Cloern, J. E., Foster, S. Q., & Kleckner, A. E. (2014). Phytoplankton primary production in the world's estuarine-coastal ecosystems. *Biogeosciences*, *11*(9), 2477–2501. https://doi.org/10.5194/bg-11-2477-2014

Concha, J. A., & Schott, J. R. (2016). Retrieval of color producing agents in Case 2 waters using Landsat 8. *Remote Sensing of Environment*, *185*, 95–107. https://doi.org/10.1016/j.rse.2016.03.018

Davison, A. C., & Hinkley, D. V. (1997). *Bootstrap methods and their applications*. Cambridge University Press. ISBN 0-521-57391-2. https://doi.org/10.1017/CBO9780511802843

Dogliotti, A., Ruddick, K., Nechad, B., & Lasta, C. (2011). Improving water reflectance retrieval from MODIS imagery in the highly turbid waters of La Plata River. In *Proceedings of the VI international conference current problems in optics of natural waters (ONW'2011), St. Petersburg, Russia, 6–9 September 2011* (pp. 3–10).

European Space Agency. (2022). Copernicus Open Access Hub. Retrieved from https://scihub.copernicus.eu/

Fenster, M. S., & Hayden, B. P. (2007). Ecotone displacement trends on a highly dynamic barrier Island: Hog Island, Virginia. *Estuaries and Coasts*, *30*(6), 978–988. https://doi.org/10.1007/BF02841389

Franz, B. A., Sean, W., Bailey, S. W., Kuring, N., & Werdell, P. J. (2015). Ocean color measurements with the Operational Land Imager on Landsat-8: Implementation and evaluation in SeaDAS. *Journal of Applied Remote Sensing*, *9*, 1–16. https://doi.org/10.1117/1.JRS.9.096070

Hamner, B., & Frasco, M. (2018). Evaluation metrics for machine learning. [R package Metrics version 0.1.4].

Hastie, T., & Tibshirani, R. (1986). *Generalized additive models*. Chapman and Hall. Hastie, T., Tibshirani, R., and Friedman, J. https://doi.org/10.1214/ss/1177013604

Hayden, B. P., Dueser, R. D., Callahan, J. T., & Shugart, H. H. (1991). Long-term research at the Virginia Coast Reserve: Modeling a highly dynamic environment. *BioScience*, *41*(5), 310–318. https://doi.org/10.2307/1311584

Ilori, C. O., Pahlevan, N., & Knudby, A. (2019). Analyzing performances of different atmospheric correction techniques for Landsat 8: Application for coastal remote sensing. *Remote Sensing*, *11*(4), 469. https://doi.org/10.3390/rs11040469

Lang, S., Cronin-Golomb, O., & Castorani, M. C. N. (2022). Satellite-based remote sensing of water clarity in the shallow coastal lagoons of Virginia 2013-2021 ver 5 [Dataset & Software]. Environmental Data Initiative. https://doi.org/10.6073/pasta/fe66683665a0133b2d831e552ecbae10

Lee, Z., Carder, K. L., & Arnone, R. A. (2002). Deriving inherent optical properties from water color: A multiband quasi-analytical algorithm for optically deep waters. *Applied Optics*, *41*(27), 5755–5772. https://doi.org/10.1364/AO.41.005755

Lee, Z., Hu, C., Shang, S., Du, K., Lewis, M., Arnone, R., & Brewin, R. (2013). Penetration of UV-visible solar radiation in the global oceans: Insights from ocean color remote sensing. *Journal of Geophysical Research: Oceans*, *118*(9), 4241–4255. https://doi.org/10.1002/jgrc.20308

Lee, Z., Shang, S., Hu, C., Du, K., Weidemann, A., Hou, W., et al. (2015). Secchi disk depth: A new theory and mechanistic model for underwater visibility. *Remote Sensing of Environment*, *169*, 139–149. https://doi.org/10.1016/j.rse.2015.08.002

Lee, Z., Shang, S., Qi, L., Yan, J., & Lin, G. (2016). A semi-analytical scheme to estimate Secchi-disk depth from Landsat-8 measurements. *Remote Sensing of Environment*, *177*, 101–106. https://doi.org/10.1016/j.rse.2016.02.033

Liu, X., Lee, Z., Zhang, Y., Lin, J., Shi, K., Zhou, Y., et al. (2019). Remote sensing of Secchi depth in highly turbid lake waters and its application with MERIS data. *Remote Sensing*, *11*(19), 2226. https://doi.org/10.3390/rs11192226

Loisel, H., Vantrepotte, V., Jamet, C., & Dat, D. N. (2013). Challenges and new advances in ocean color remote sensing of coastal waters. In *Topics in oceanography*. https://doi.org/10.5772/56414

Luis, K. M. A., Rheuban, J. E., Kavanaugh, M. T., Glover, D. M., Wei, J., Lee, Z., & Doney, S. C. (2019). Capturing coastal water clarity variability with Landsat 8. *Marine Pollution Bulletin*, *145*, 96–104. https://doi.org/10.1016/j.marpolbul.2019.04.078

Manzo, C., Bresciani, M., Giardino, C., Braga, F., & Bassani, C. (2015). Sensitivity analysis of a bio-optical model for Italian lakes focused on Landsat-8, Sentinel-2 and Sentinel-3. *European Journal of Remote Sensing*, *48*(1), 17–32. https://doi.org/10.5721/EuJRS20154802

Masek, J., Ju, J., Roger, J., Skakun, S., Claverie, M., & Dungan, J. (2018). Harmonized Landsat/Sentinel-2 products for land monitoring. In *Presented at the IGARSS 2018 - 2018 IEEE international geoscience and remote sensing symposium* (pp. 8163–8165). https://doi.org/10.1109/IGARSS.2018.8517760

Maul, G. A., & Duedall, I. W. (2019). Demography of coastal populations. In C. W. Finkl & C. Makowski (Eds.), *Encyclopedia of coastal science. Encyclopedia of earth sciences series*. Springer. https://doi.org/10.1007/978-3-319-93806-6_115

McGlathery, K., Anderson, I., & Tyler, A. (2001). Magnitude and variability of benthic and pelagic metabolism in a temperate coastal lagoon. *Marine Ecology Progress Series*, *216*, 1–15. https://doi.org/10.3354/meps216001

McGlathery, K., & Christian, R. (2020). Water quality sampling-integrated measurements for the Virginia Coast, 1992-2019. Virginia Coast Reserve Long-Term Ecological Research Project Data Publication knb-lter-vcr.247.14. https://doi.org/10.6073/pasta/db7f8fe720ddfcdfab1352adc9c22702

Mélin, F. (2022). Validation of ocean color remote sensing reflectance data: Analysis of results at European coastal sites. *Remote Sensing of Environment*, *280*, 113153. https://doi.org/10.1016/j.rse.2022.113153

Morel, A., Antoine, D., & Gentili, B. (2002). Bidirectional reflectance of oceanic waters: Accounting for Raman emission and varying particle scattering phase function. *Applied Optics*, *41*(30), 6289–6306. https://doi.org/10.1364/AO.41.006289

Morel, A., & Bélanger, S. (2006). Improved detection of turbid waters from ocean color sensors information. *Remote Sensing of Environment*, *102*(3–4), 237–249. https://doi.org/10.1016/j.rse.2006.01.022

Nardin, W., Larsen, L., Fagherazzi, S., & Wiberg, P. (2018). Tradeoffs among hydrodynamics, sediment fluxes and vegetation community in the Virginia Coast Reserve, USA. *Estuarine, Coastal and Shelf Science*, *210*, 98–108. https://doi.org/10.1016/j.ecss.2018.06.009

National Aeronautics and Space Administration, & Ocean Biology Processing Group. (2022). SeaDAS 8.1.0 [Software]. Retrieved from https://seadas.gsfc.nasa.gov/downloads/

Orth, R. J., Lefcheck, J. S., McGlathery, K. S., Aoki, L., Luckenbach, M. W., Moore, K. A., et al. (2020). Restoration of seagrass habitat leads to rapid recovery of coastal ecosystem services. *Science Advances*, *6*(41), eabc6434. https://doi.org/10.1126/sciadv.abc6434

Orth, R. J., Moore, K. A., Marion, S. R., Wilcox, D. J., & Parrish, D. B. (2012). Seed addition facilitates eelgrass recovery in a coastal bay system. *Marine Ecology Progress Series*, *448*, 177–195. https://doi.org/10.3354/meps09522

Page, B. P., Olmanson, L. G., & Mishra, D. R. (2019). A harmonized image processing workflow using Sentinel-2/MSI and Landsat-8/OLI for mapping water clarity in optically variable lake systems. *Remote Sensing of Environment*, *231*, 111284. https://doi.org/10.1016/j.rse.2019.111284

Pahlevan, N., Chittimalli, S. K., Balasubramanian, S. V., & Vellucci, V. (2019). Sentinel-2/Landsat-8 product consistency and implications for monitoring aquatic systems. *Remote Sensing of Environment*, *220*, 19–29. https://doi.org/10.1016/j.rse.2018.10.027

Parker, S., & Crichton, G. (2011). *Effects of global climate change at the Virginia Coast Reserve* (pp. iii–v). The Nature Conservancy. Retrieved from https://www.conservationgateway.org/ConservationByGeography/NorthAmerica/UnitedStates/virginia/Documents/Effects%20of%20Global%20Climate%20Change%20at%20VCR%202011%20FINAL.pdf

Pesce, M., Critto, A., Torresan, S., Giubilato, E., Santini, M., Zirino, A., et al. (2018). Modelling climate change impacts on nutrients and primary production in coastal waters. *Science of the Total Environment*, *628–629*, 919–937. https://doi.org/10.1016/j.scitotenv.2018.02.131

Peterson, K. T., Sagan, V., & Sloan, J. J. (2020). Deep learning-based water quality estimation and anomaly detection using Landsat-8/Sentinel-2 virtual constellation and cloud computing. *GIScience & Remote Sensing*, *57*(4), 510–525. https://doi.org/10.1080/15481603.2020.1738061

Pitarch, J. (2020). A review of Secchi's contribution to marine optics and the foundation of Secchi disk science. *Oceanography*, *33*(3), 26–37. https://doi.org/10.5670/oceanog.2020.301

Preisendorfer, R. W. (1986). Secchi disk science: Visual optics of natural waters1. *Limnology & Oceanography*, *31*(5), 909–926. https://doi.org/10.4319/lo.1986.31.5.0909

QGIS.org. (2020). QGIS Geographic Information System [Software]. QGIS Association. Retrieved from http://qgis.osgeo.org

R Core Team. (2022). R: A language and environment for statistical computing [Software]. R Foundation for Statistical Computing. Retrieved from https://www.R-project.org/

Reynolds, L. K., Waycott, M., McGlathery, K. J., & Orth, R. J. (2016). Ecosystem services returned through seagrass restoration. *Restoration Ecology*, *24*(5), 583–588. https://doi.org/10.1111/rec.12360

Royal Belgian Institute of Natural Sciences, & The Remote Sensing and Ecosystem Modelling Team. (2022). ACOLITE V20220222.0 [Software]. Retrieved from https://odnature.naturalsciences.be/remsem/software-and-data/acolite

Safak, I., Wiberg, P. L., Richardson, D. L., & Kurum, M. O. (2015). Controls on residence time and exchange in a system of shallow coastal bays. *Continental Shelf Research*, *97*, 7–20. https://doi.org/10.1016/j.csr.2015.01.009

Sallenger, A. H., Doran, K. S., & Howd, P. A. (2012). Hotspot of accelerated sea-level rise on the Atlantic coast of North America. *Nature Climate Change*, *2*(12), 884–888. https://doi.org/10.1038/nclimate1597

Shi, W., Wang, M., & Jiang, L. (2013). Tidal effects on ecosystem variability in the Chesapeake Bay from MODIS-Aqua. *Remote Sensing of Environment*, *138*, 65–76. https://doi.org/10.1016/j.rse.2013.07.002

Sullivan, H., Bolgrien, D., Brown, C., Harwell, L., Kiddon, J., Pelletier, M., et al. (2021). National Coastal Condition Assessment: A collaborative survey of the nation's estuaries and Great Lakes waters. United States Environmental Protection Agency. Retrieved from https://www.epa.gov/system/files/documents/2021-09/nccareport_final_2021-09-01.pdf

The MathWorks Inc. (2022). MATLAB version: 9.9.0 (R2020b) [Software]. The MathWorks Inc. Retrieved from https://www.mathworks.com

Trombetta, T., Vidussi, F., Mas, S., Parin, D., Simier, M., & Mostajir, B. (2019). Water temperature drives phytoplankton blooms in coastal waters. *PLoS One*, *14*(4), e0214933. https://doi.org/10.1371/journal.pone.0214933

Turner, J. S., St-Laurent, P., Friedrichs, M. A. M., & Friedrichs, C. T. (2021). Effects of reduced shoreline erosion on Chesapeake Bay water clarity. *Science of the Total Environment*, *769*, 145157. https://doi.org/10.1016/j.scitotenv.2021.145157

Ummenhofer, C. C., & Meehl, G. A. (2017). Extreme weather and climate events with ecological relevance: A review. *Philosophical Transactions of the Royal Society B: Biological Sciences*, *372*(1723), 20160135. https://doi.org/10.1098/rstb.2016.0135

U.S. Geological Survey. (2022). Earth Explorer. Retrieved from https://earthexplorer.usgs.gov/

Vanhellemont, Q. (2019). Adaptation of the dark spectrum fitting atmospheric correction for aquatic applications of the Landsat and Sentinel-2 archives. *Remote Sensing of Environment*, *225*, 175–192. https://doi.org/10.1016/j.rse.2019.03.010

Vanhellemont, Q. (2020). Sensitivity analysis of the dark spectrum fitting atmospheric correction for metre-and decametre-scale satellite imagery using autonomous hyperspectral radiometry. *Optics Express*, *28*(20), 29948–29965. https://doi.org/10.1364/OE.397456

Vanhellemont, Q., & Ruddick, K. (2018). Atmospheric correction of metre-scale optical satellite data for inland and coastal water applications. *Remote Sensing of Environment*, *216*, 586–597. https://doi.org/10.1016/j.rse.2018.07.015

Wei, J., Lee, Z., Garcia, R., Zoffoli, L., Armstrong, R. A., Shang, Z., et al. (2018). An assessment of Landsat-8 atmospheric correction schemes and remote sensing reflectance products in coral reefs and coastal turbid waters. *Remote Sensing of Environment*, *215*, 18–32. https://doi.org/10.1016/j.rse.2018.05.033

Werdell, P. J., & McClain, C. R. (2019). Satellite remote sensing: Ocean color. In *Encyclopedia of ocean sciences* (3rd ed., pp. 443–455). Academic Press. https://doi.org/10.1016/B978-0-12-409548-9.10817-6

Windle, A. E., Evers-King, H., Loveday, B. R., Ondrusek, M., & Silsbe, G. M. (2022). Evaluating atmospheric correction algorithms applied to OLCI Sentinel-3 data of Chesapeake Bay waters. *Remote Sensing*, *14*(8), 1881. https://doi.org/10.3390/rs14081881

Wood, S. N. (2017). *Generalized additive models: An Introduction with R, Second Edition* (2nd ed.). Chapman and Hall/CRC. https://doi.org/10.1201/9781315370279

Yang, W., Matsushita, B., Chen, J., Yoshimura, K., & Fukushima, T. (2014). Application of a semianalytical algorithm to remotely estimate diffuse attenuation coefficient in turbid inland waters. *IEEE Geoscience and Remote Sensing Letters*, *11*(6), 1046–1050. https://doi.org/10.1109/LGRS.2013.2284343

References From the Supporting Information

Richardson, D., Porter, J., Oertel, G., Zimmerman, R., Carlson, C., Overman, K., & Carlson, C. (2018). *Integrated topography and bathymetry for the eastern shore of Virginia ver 10*. Environmental Data Initiative. https://doi.org/10.6073/pasta/63a22558d6650fae8232b6a8814a90d5